AADE-23-NTCE-047

Identifying Lost-Circulation Zones from Shear Wave Slowness in Volve Field-North Sea using Machine Learning

S. M. Kholy, and Hunjoo P. Lee, Oklahoma State University

Abstract

Shear wave has a unique character of splitting into two orthogonal waves when it encounters a discontinuity in the media. Based on this phenomenon, the shear wave transit time (DTS) could be utilized to identify lost-circulation zones along the wellbore. Therefore, the objective of this study is to develop a method to identify potential mud loss zones by improving the accuracy of DTS prediction using machine learning models based on conventional well logs.

Drilling reports of two adjacent offshore wells in the Volve field indicate mud loss events in the Ty formation in one well (11A) but not in the other well (1A). Three machine learning algorithms, Linear Regression (LR), Artificial Neural Network (ANN), and Decision Tree (DT), are trained from both wells. To identify fractured layers of possible mud loss events, we evaluated the discrepancy between the DTS predictions from the two models trained from 11A and 1A. Shear splitting signatures, larger DTS discrepancy, are identified at the depth of Ty formation from the DT and ANN models, which agrees with the drilling reports, while the LR model has shown less accuracy. The developed predictive models from this study can help detect formations of potential mud loss incidents and accurately estimate the mechanical properties of subsurface formations, which are critical inputs for drilling simulators.

Introduction

Lost circulation is a major problem in oil and gas well drilling, especially in highly permeable, naturally fractured, or cavernous formations (Rabia, 2002). This may lead to severe issues in drilling operations, such as drill string sticking, wellbore instability, bit wear, or blowout depending on the mud loss percentage, consequently leading to an increase in the drilling downtime (Ameen, 2014). The most accurate way to detect lost circulation is to monitor the mud return level and compare it to the mud tank level (Rabia, 2002). Recently, several studies incorporated artificial intelligence to predict mud loss volume by developing supervised machine learning (ML) models based on the drilling parameters, such as weight on bit, torque, yield point, pump pressure, and flow rate. These studies include the cases of the Dammam formation in Iraq (Al-Hameedi et al., 2017) and the Asmari formation in Iran using Artificial Neural Network (ANN) models (Moazzeni et al., 2010; Toreifi et al., 2014). In addition, some studies suggested that incorporating the geomechanical data along with the drilling parameters helps in improving the ANN prediction accuracy for mud losses (Jahanbakhshi et al., 2014; Jahanbakhshi and Keshavarzi, 2015). Also, Ahmed et al. (2020) developed ANN and functional network models to predict the mud loss volume based on drilling data from High-Pressure High Temperature (HPHT) wells.

Shear wave transit time (DTS) has been utilized in many subsurface engineering applications to identify fractures, formation layering, in-situ stress changes, and faults in subsurface formations (Will et al., 2005). This is because of the unique nature of the shear wave, splitting into two polarized orthogonal waves of different velocities when it travels through an anisotropic medium so that the faster wave propagates along the fracture plane, and the slower wave propagates perpendicular to it (Tillotson et al., 2012). The velocity difference between the two split waves can be utilized to quantify the degree of anisotropy in a medium (Tillotson et al. 2012; Katsuki et al., 2019).

Several empirical equations have been developed to predict the shear wave velocity (V_s), i.e., the inverse of DTS, from the compressional wave velocity (V_p) for homogeneous rocks due to the strong correlation between the two properties. Castagna et al. (1985) developed a linear correlation for mud rocks (Equation 1), while Brocher (2005) suggested a polynomial correlation for a wide variety of lithologies (Equation 2) as shown below:

$$V_s = \frac{V_p - 1.36}{1.16} \quad (1)$$

$$V_s = 0.7858 - 1.2344V_p + 0.7949V_p^2 - 0.1238V_p^3 + 0.006V_p^4 \quad (2)$$

The compressional transit time (DTC) and DTS, in µs/ft, are equal to $304.8/V_p$ and $304.8/V_s$, respectively., and V_p and V_s are in Km/s.

Several studies tried to indirectly correlate mud loss volume to the filtration rate. Jeirani and Mohebbi (2006) utilized statistics to develop empirical equations for filtration rate and mud cake permeability as functions of static filtration data, e.g., time, pressure drop, H_2O wt%, and NaCl wt%. Recent studies

proposed ML models to predict DTS from either drilling parameters or conventional well logs. Wood (2020) developed a Transparent Open Box (TOB) model to predict DTS of the Bakken shale formation in the Williston basin from conventional well logs. Gowida and Elkatatny (2020) developed an ANN model to predict DTS of carbonate rocks from drilling parameters, while Muqtadir et al. (2019) focused on tight sandstones using an ANN model. Similarly, Roy et al. (2022) and Rajabi et al. (2022) compared the prediction accuracy of several hybrid ML models that predict DTS from well logs. However, these studies did not consider the possibility of utilizing DTS to identify the loss of circulation zones.

Therefore, the objective of our study is developing a new method to identify zones of possible mud loss events based on DTS measurements and predictions. This is achieved by developing supervised ML models including Linear Regression (LR), ANN, and Decision Tree (DT) that predict DTS from conventional well logs. These models were developed separately for two adjacent wells in the Volve offshore oilfield located in the Norwegian North Sea. The first well suffered from severe mud losses across the Ty formation, while the same formation in the second well had no mud losses. Afterward, the difference between the predicted DTS from the mud loss and the no mud loss models was utilized to identify potential lost circulation zone(s) for several test cases.

Review on Volve Field and Available Data

Volve field is an offshore oilfield located in the southern Norwegian North Sea, where the water depth is approximately 300 ft. The main producing zone is the Hugin formation, a heavily faulted structure formed of sandstone with layers of claystone. The cap rock above the Hugin formation is the Draupne formation, which is claystone. In this field, the wells are drilled from a jack-up rig, which is made of 15 surface slots. From each slot, a vertical hole is drilled to a depth of approximately 2,500 ft, then a set of multi-laterals are deployed and landed at Hugin formation to maximize the drainage area of the reservoir as shown in Figure 1a. In this study, the drilling reports of wells 11A, 1A, and 1B in the Volve field have been evaluated to locate lost circulation zones. The report of well 11A indicated that the Ty formation, predominantly sandstone with layers of limestone and claystone, is the lost circulation zone. While the reports of the other two wells did not show any mud loss for the same formation, where the Ty formation top in well 1A is horizontally 2,330 ft apart from the Ty formation top in well 11A as shown in Figure 1b.

The conventional well logs of these three wells have been collected including true vertical depth (TVD), gamma ray (GR), bulk density (RHOB), neutron porosity (PHIN), DTC, and DTS as shown in Figure 2. The acoustic logs (i.e., DTC and DTS) were measured using a quadrupole acoustic logging while drilling (LWD) tool, which is made of several quadrupole transmitters that are capable of reducing the waves interference during drilling and strengthening the shear waveform (Chen, 1989). The Ty formation in well 11A indicates that the DTS values are approximately 150 μs/ft higher than the values in well 1A. This relative slowness across Ty formation in well 11A is possibly due to the presence of natural fractures.

To verify the presence of fractured zones, both the DTC and DTS data were plotted versus each other for each well separately. Then, they were compared to Castagna et al. (1985) and (Brocher, 2005) models that were developed for isotropic porous media as discussed earlier in Equations 1 and 2. Figure 3 shows this comparison, and it can be clearly seen that there is a distinct feature, a range of data below the curves of the isotropic models, in well 11A (Figure 3b) compared to wells 1A (Figure 3a) and 1B (Figure 3c). The data set that fall out of the isotropic model, highlighted by a blue circle in Figure 3b, are mostly across the Ty formation (marked by red crosses) in well 11A. The values in this highlighted zone are generally higher, by approximately 100 μs/ft, than the estimated values by the isotropic models and the measured values from the same formation in the other two wells.

ML Models Development

Three ML models were considered in this study including LR, ANN, and DT models. The ML models were trained by well logging data of well 1A and 11A, while well logs of well 1B were used for validation. The development for each of these models follows the steps: (1) Well logs pre-processing, (2) Features selection, and (3) ML models Architecture.

Well logs pre-processing

In this step, all the outliers are excluded from each of the conventional well logs including the nulls and negative values. Also, the GR log was bounded by an upper limit of 150 to eliminate the spikes of high uranium content (Koizumi 1988; Rodolfo et al. 2010), which improved the correlation evaluation between the GR and the DTS as will be discussed in features selection step. After pre-processing, the total number of data points is 10,199 for well 1A, 11,084 for well 11A., and 2,813 for well 1B.

Features Selection

The correlation between the DTS and each of the conventional well logs was evaluated to select the well logs that have strong correlation with DTS. The selected well logs represent the inputs (i.e., features) for the ML models. Pearson's correlation coefficient, *r*, was utilized for this evaluation as,

$$r = \frac{\sum_{i=1}^{m}\left(X_i - \overline{X}\right)\left(\mathrm{DTS}_i - \overline{\mathrm{DTS}}\right)}{\sqrt{\sum_{i=1}^{m}\left(X_i - \overline{X}\right)^2 \sum_{i=1}^{m}\left(\mathrm{DTS}_i - \overline{\mathrm{DTS}}\right)^2}} \quad (3)$$

where *m* is the number of data points, *X* is the evaluated feature, $\bar{X}$ is the mean of the evaluated feature, and $\overline{DTS}$ is the mean of DTS values. A strong correlation is an *r* value that is greater than or equal to 0.5 or a value of less than or equal to –0.5.

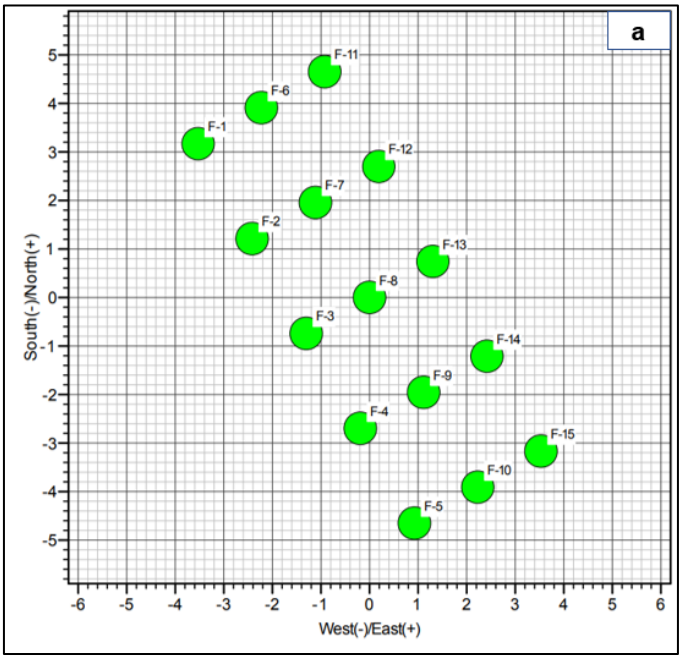

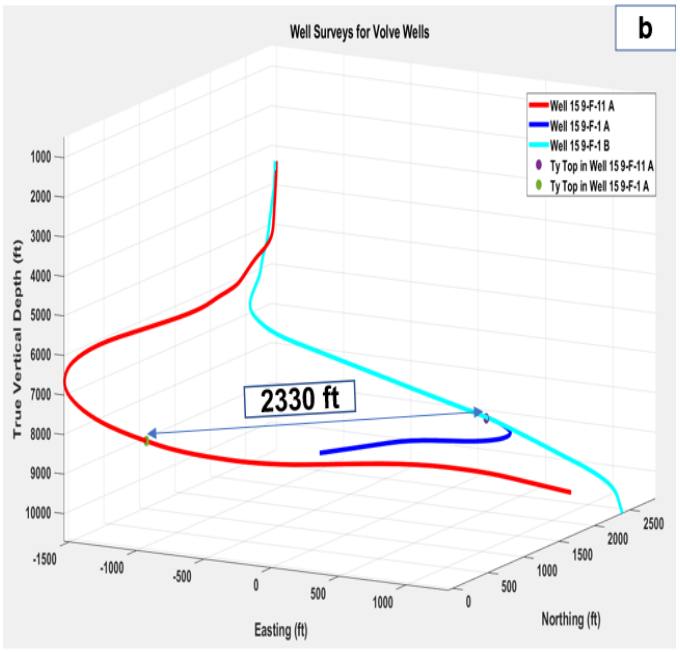

Figure 1: (a) Surface well slots from which all the wells in the Volve field are originated. (b) Well profiles for wells 11A, 1A, and 1B. The Ty formation top in well 11A is 2,330 ft apart from the top of the same formation in wells 1A and 1B.

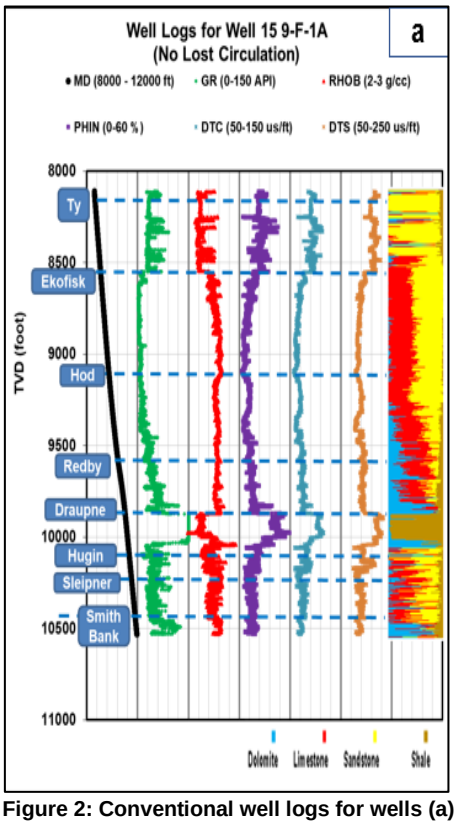

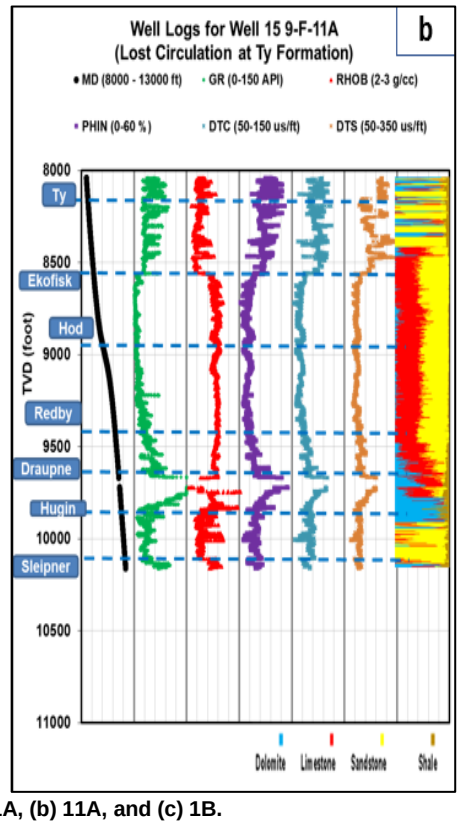

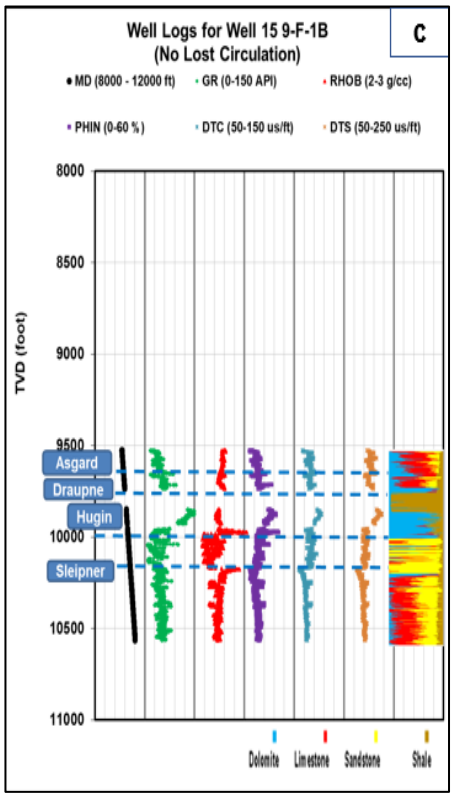

Figure 2: Conventional well logs for wells (a) 1A, (b) 11A, and (c) 1B.

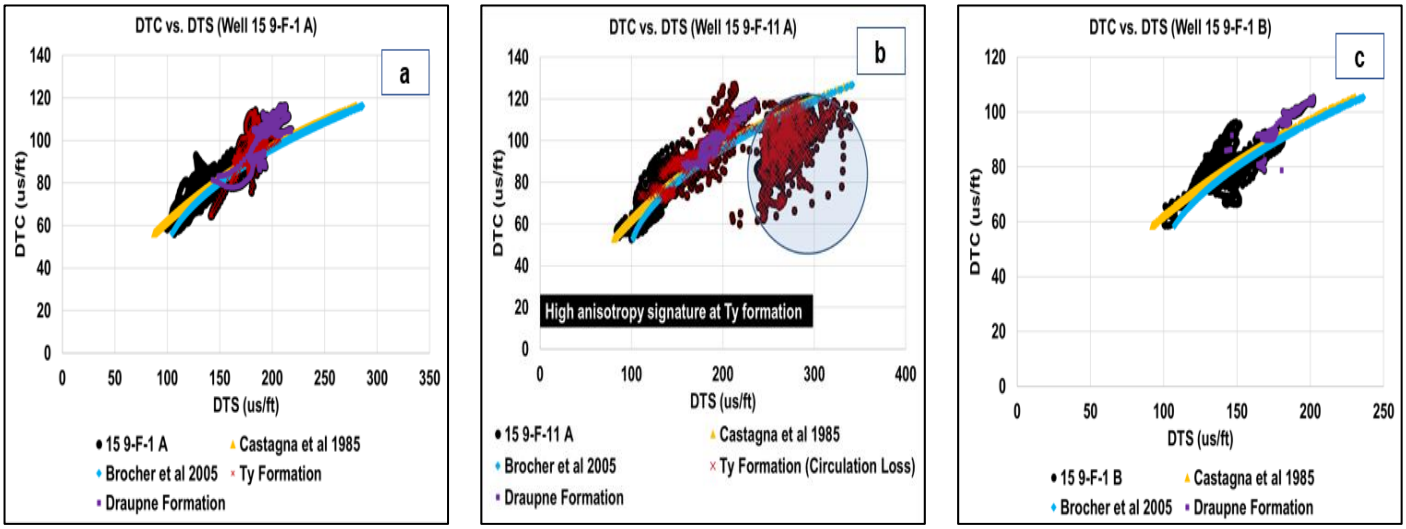

Figure 3: The acoustic data of each of the wells were compared to isotropic models to identify any troublesome zones. (a)Well 1A comparison. (b)Well 11A comparison shows that Ty formation, which suffered from mud loss, has significantly higher DTS values than the normal trend models. (c)Well 1B comparison.

Figure 4 summarizes the correlation between DTS and each of the conventional well logs for well 1A. DTC has the strongest direct correlation with DTS with an *r* value of 0.93. PHIN and GR have strong direct correlations with DTS with *r* values of 0.86 and 0.6, respectively. On the other hand, RHOB and TVD have inverse correlations with DTS with *r* values of –0.68 and –0.25, respectively. Finally, the resistivity (Rt) has the weakest correlation with DTS with *r* value of 0.016. Therefore, DTC, PHIN, GR, RHOB, and TVD were selected as inputs, while Rt was excluded. The *r* value for TVD is greater than –0.5, but it was selected as an input to incorporate the confining stress effect along with the RHOB to the developed models as was discussed in Kholy and Lee (2022).

Similarly, the correlation coefficients were assessed for well 11A as shown in Figure 5. The neuron porosity showed the strongest correlation with DTS, unlike well 1A where DTC has the strongest correlation. This could be related to the relatively high permeability of Ty formation in well 11A, compared to well 1A, due to the possible existence of natural fractures (Kozeny 1927; Carman 1937; Panda and Lake 1994; Costa 2006). The same inputs were selected for the ML models development as in well 1A since they showed strong correlation with DTS with *r* values of 0.85, 0.83, –0.66, 0.54, –0.44 for PHIN, DTC, RHOB, GR, and TVD, respectively.

ML Models Architecture

The next step is to architect the ML models: LR, ANN, and DT. Generally, the architecture for each model is selected to achieve minimum difference between the actual DTS and the predicted DTS from the model. This difference can be evaluated using the Root Mean Square Error (RMSE) as:

$$RMSE = \sqrt{\frac{1}{2m}\sum_{i=1}^{m}\left(\mathrm{DTS}_i - \mathrm{DTS}_{h_i}\right)^2} \quad (4)$$

where DTS_h is the predicted DTS from the hypothesis function.

The Linear Regression (LR) Model

The LR model is the simplest model in terms of the number of the parameters (θ) in the hypothesis function. In this study, we have five inputs, and hence we should have six parameters in the LR's hypothesis function as in Equation 5:

$$\mathrm{DTS}_h = \theta_0 + \theta_1 TVD + \theta_2 GR + \theta_3 RHOB + \theta_4 PHIN + \theta_5 DTC \quad (5)$$

The parameters in the hypothesis function were solved analytically using Equation 6 (Bishop, 2006):

$$\theta = (X^T X)^{-1} X^T DTS \quad (6)$$

where *X* is a matrix that is made of six columns (i.e., each input is defined in a column and the sixth column is the bias column which is made of ones), the superscript "*T*" represents the transpose of the matrix, while the superscript "–1" represents the matrix inverse.

For well 1A, the hypothesis parameters θ_0, θ_1, θ_2, θ_3, θ_4, and θ_5 were estimated to be 58.677, -0.0087, 0.0824, 11.723, 0.1667, 1.683, respectively. These parameters yield an RMSE value of 4.75 µs/ft for this model. Similarly, the LR model was developed for well 11A with an RMSE value of 13.19 µs/ft with hypothesis parameters of 270.9, –0.02846, 0.17202, 5.7625, 1.9024, and 1.088.

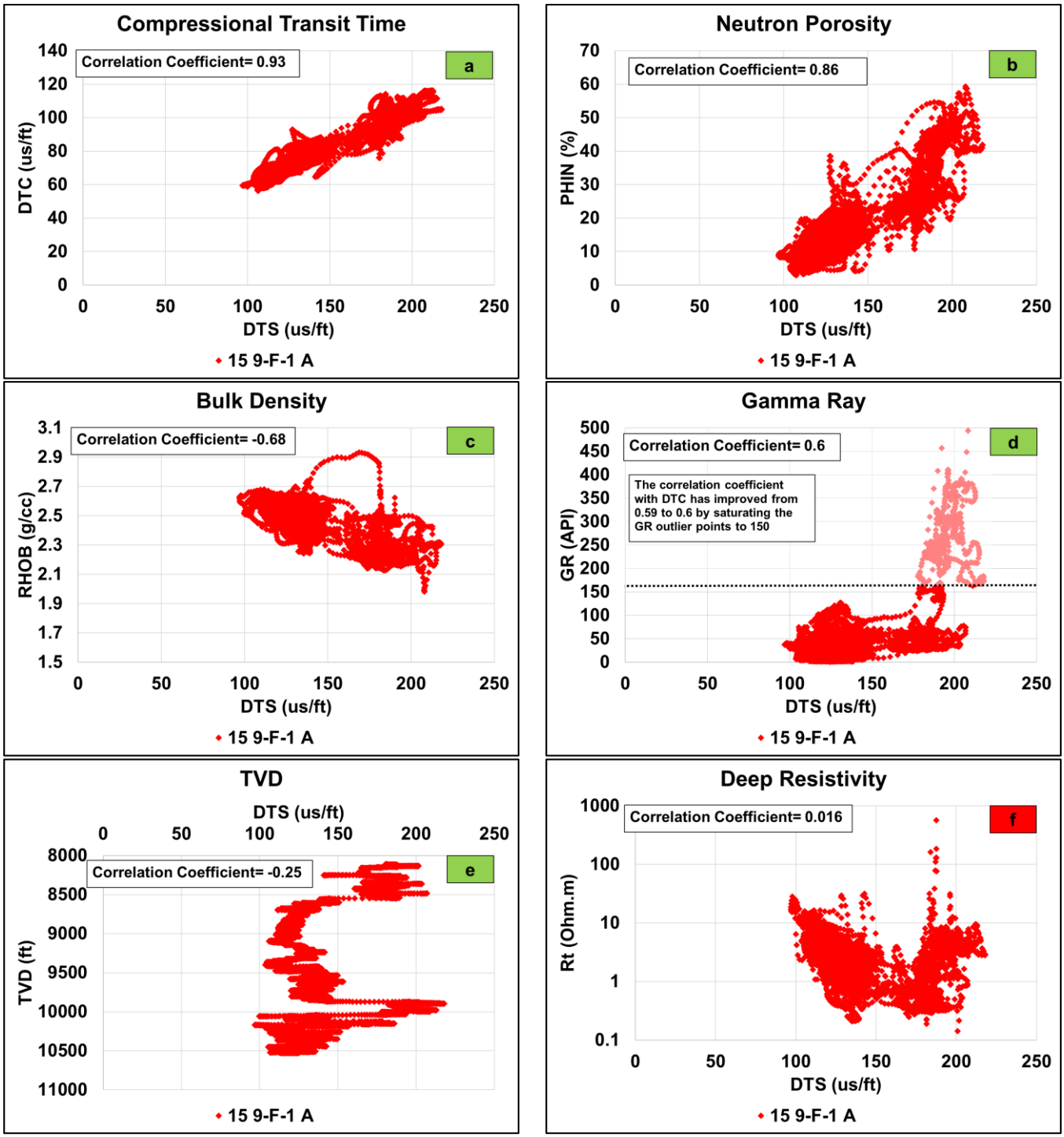

Figure 4: The correlation between DTS and each of the conventional well logs for well 1A from the strongest to the weakest. The green label means the well log was selected for model development, while the red means the well log was not selected. (a)DTC. (b)PHIN. (c)RHOB. (d)GR. (e)TVD. (f)R_t.

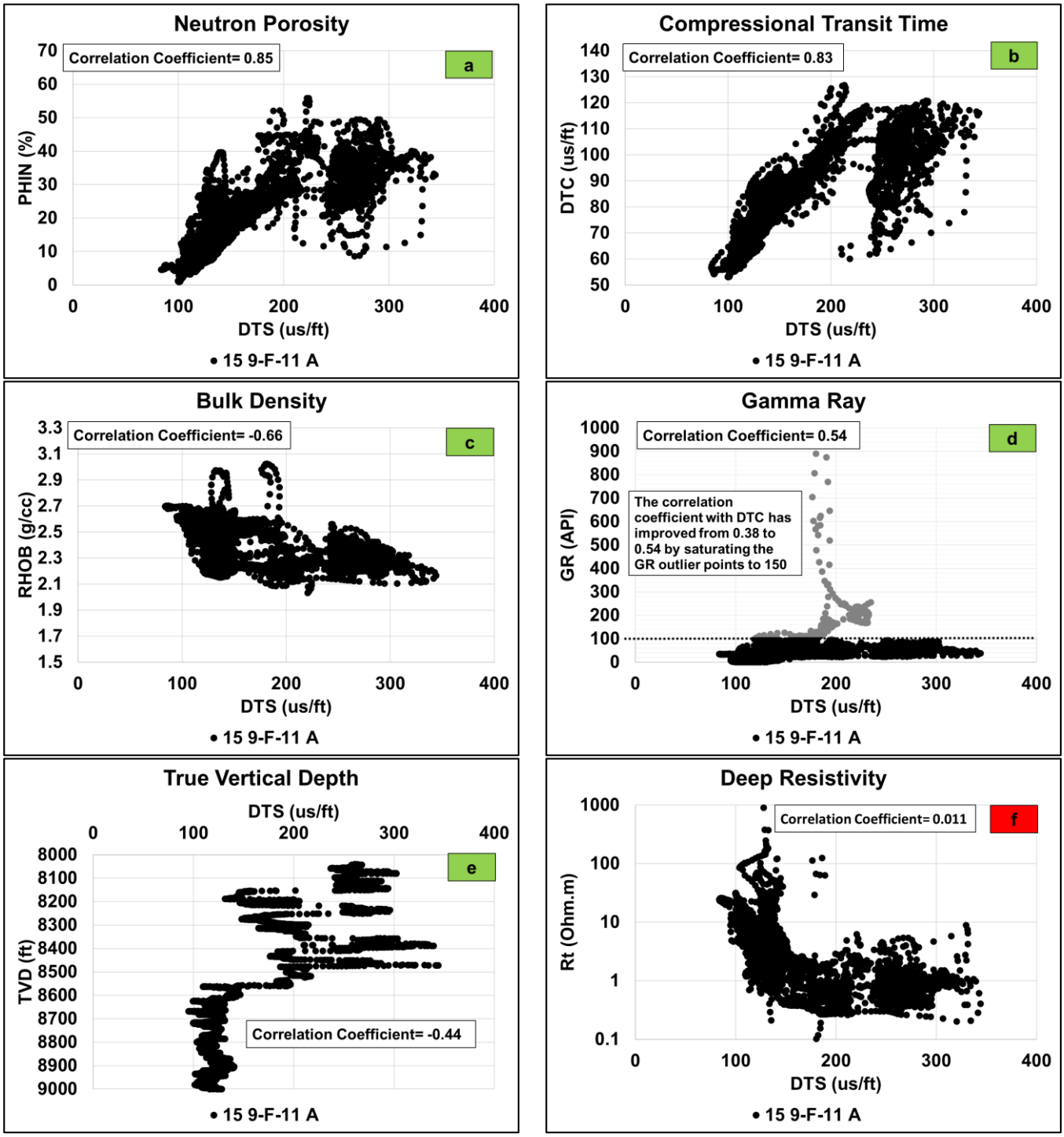

Figure 5: The correlation between DTS and each of the conventional well logs for well 11A from the strongest to the weakest. The green label means the well log was selected for model development, while the red means the well log was not selected. (a)PHIN. (b)DTC. (c)RHOB. (d)GR. (e)TVD. (f)R_t.

The Artificial Neural Network (ANN) Model

The ANN model has been utilized to predict and to solve several oil and gas challenges over the last decade. In this study, we used ANN model to predict the DTS by finding the optimum weights that connect the neurons in the hidden layers together to achieve the lowest difference between the actual and the predicted DTS. The first step is to normalize both the input and the output variables to aid the model converges to the optimum weights with,

$$X_n = \frac{X - \mu}{\sigma} \tag{7}$$

where μ represents the mean of the variable, and σ is its standard deviation. Also, the subscript "n" means it is a normalized variable.

After that, the dataset was divided into training data representing 70%, and the other 30% of the dataset for validation. Next step was to select the hyperparameters of the model including neurons and hidden layers. Two hidden layers were selected, and the number of neurons per hidden layer was optimized to avoid model overfitting. 12 neurons per hidden layer yields the lowest validation RMSE of 5.94 µs/ft as shown in Figure 6. Figure 7 shows the optimum architecture of the ANN model, which is made of 1 input layer, 2 hidden layers with 12 neurons each, and 1 output layer.

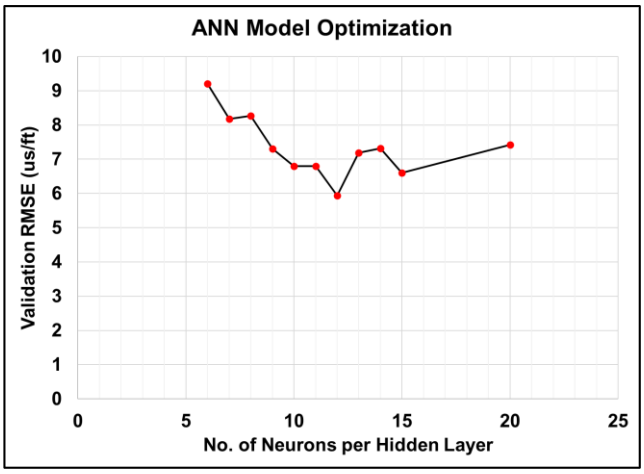

Figure 6: ANN Model Optimization

The feedforward back propagation method estimates the cost function, which should be minimized to attain the values of the optimum weights of the ANN model as described by (Bishop, 2006),

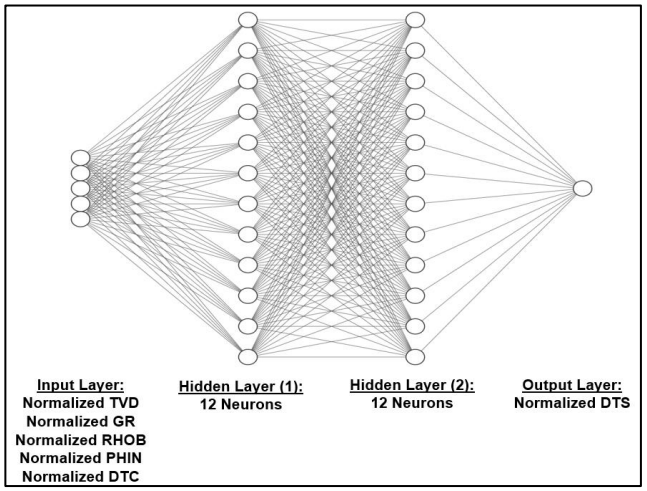

Figure 7: ANN Optimum Architecture

$$J(\theta) = \frac{-1}{m}\left[\sum_{i=1}^{m} \mathrm{DTS}_i \log \mathrm{DTS}_{h_i} + (1 - \mathrm{DTS}_i)\log\left(1 - \mathrm{DTS}_{h_i}\right)\right] + \frac{\lambda}{2m}\left[\sum_{l=1}^{L-1}\sum_{i=1}^{S_l}\sum_{j=1}^{S_{l+1}}\left(\theta_{ji_l}\right)^2\right] \tag{8}$$

where L is the total number of layers, S_l is the number of neurons in the layer "l", θ_{ji} is a weighting term corresponding to the neuron "s" in the layer "l", and λ represents the regularization term, which is equal to 10.

The ANN model training results yield RMSE values of 2.19 µs/ft and 5.27 µs/ft for wells 1A and 11A, respectively.

The Decision Tree (DT) Regression Model

The DT regression is a commonly utilized supervised ML model. Figure 8 represents a simple diagram of the DT model showing the main terms of the model. The root node represents the start point of the tree, and it contains the whole training dataset. The branched nodes from the decision node are called the child nodes to that of the parent decision node. The tree is built by splitting the training datasets into subsets by generating several splitting conditions at each of the root nodes and the decision nodes based on the values of the input variables.

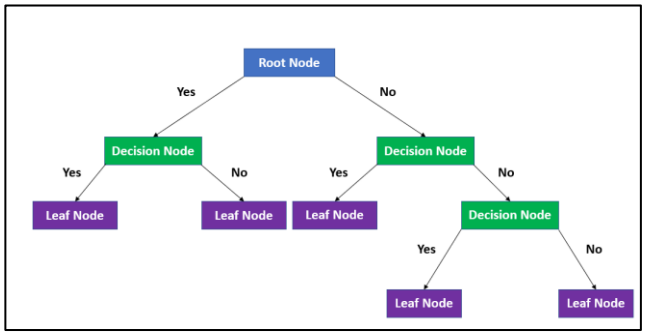

Figure 8: A Typical Diagram of a DT Model

The best splitting condition at each root or decision node represents the one that yields the lowest variance at that node. This is achieved by calculating the variance at each child node as (Bishop, 2006),

$$Variance = \frac{\sum_{i=1}^{N}(X_i - \mu)^2}{N} \quad (9)$$

where N is the number of datapoints at a child node. Then, the weighted average variance of the child nodes is calculated.

The splitting of the tree stops at the leaf node, when the minimum leaf size is achieved, where the leaf size represents the number of data points at a node. First, the dataset is divided into two: 70% for training and 30% for validation. The validation dataset was utilized to optimize the minimum leaf size, so that a minimum leaf size of 4 yields the lowest validation RMSE value of 4.89 µs/ft as shown in Figure 9.

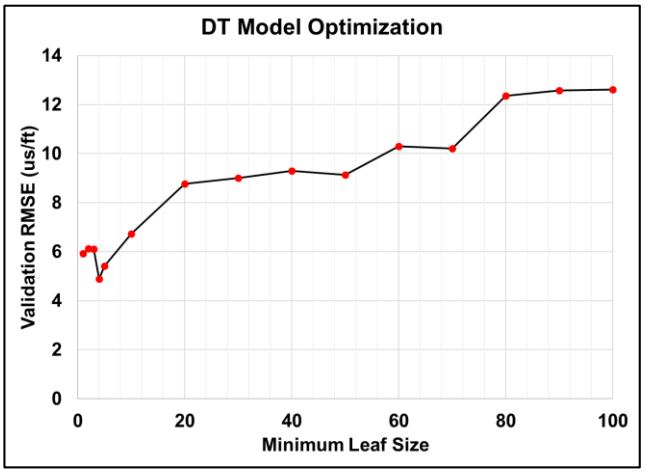

Figure 9: DT Model Optimization

The DT model training results yield RMSE values of 0.69 µs/ft and 1.82 µs/ft for wells 1A and 11A, respectively.

Figure 11 shows a comparison between the actual DTS and the predicted DTS from the 3 trained models for wells 1A and 11A. The models can be ranked in terms of prediction accuracy as the DT model, then the ANN model, and finally the LR model.

Validation and Discussion

After training the 3 ML models, the validation was conducted on wells 1A, 1B, and 11A to evaluate the accuracy of each model in identifying potential lost circulation zones, thief zones. This was done by subtracting the predicted DTS from the mud loss model (trained by well 11A dataset) out of the predicted DTS from the no mud loss model (trained by well 1A dataset). If this difference is zero then the formation is likely unfractured with no mud loss, while a high positive difference likely indicates a fractured zone. In this study, since the average of the actual DTS difference in Ty formation, DTS in well 11A minus the DTS in well 1A, was 130 µs/ft, we assumed it is a fractured zone if the predicted DTS difference is above this value. Other positive or negative DTS differences below 130 µs/ft might be related to other lithological features including the heterogeneity of reservoir compaction/stiffness in the same formation (Gutierrez 2017). Also, the prediction inaccuracy of the ML models could be another source of uncertainty in the small variances of DTS differences.

For well 1A that had no mud loss, Figure 10a shows the predicted DTS difference from the 3 ML models. The LR model showed DTS difference of almost zero for all depths except for the Draupne formation (from 9,872 TVD ft to 10,040 TVD ft), where the LR model predicted a positive DTS difference of approximately 50 µs/ft, opposite trend compared to the other two models. The ANN model predicted zero DTS difference for most of the formations. However, it showed negative DTS difference values for the Draupne and the Ekofisk formations of –75 µs/ft and –95 µs/ft, respectively, which could presumably due to the over-compaction as discussed above since the formation is dominantly claystone. The DT model also predicted a negative DTS difference of –50 µs/ft across the Draupne formation. However, the DT model indicated positive DTS difference in the Ekofisk and lower Ty formations suggesting further investigation is necessary for these zones.

Figure 10b shows the predicted DTS difference from the 3 ML models for well 11A, which had severe mud loss across the Ty formation (from 8,047 TVD ft to 8,513 TVD ft) based on the drilling reports. However, the LR model did not predict any possible mud loss zones across the Ty formation with a DTS difference of almost zero, while the ANN and the DT models successfully predicted four fractured zones by showing a DTS difference of close to or greater than 130 µs/ft. The ANN and the LR models also predicted high DTS differences in the Draupne formation. On the other hand, the DT model did not show the same trend, which suggests that the DT model may have greater uncertainties and the ANN model is more accurate in detecting possible lost circulations zones. Future investigation with more lithology information is required to validate this finding.

For a further validation, we estimated the DTS differences of well 1B, a subset well of 1A, that did not experience any mud loss in the deeper layers. The DTS difference values are nearly zero for all formations from the LR model. For the ANN and DT model, there are some negative DTS difference values in the Draupne formation (ANN) and positive values in the Asgard formation (DT). However, there is no clear formation that both models show high positive DTS differences (i.e., above 130 µs/ft) in these deeper layers to suggest highly fractured layers.

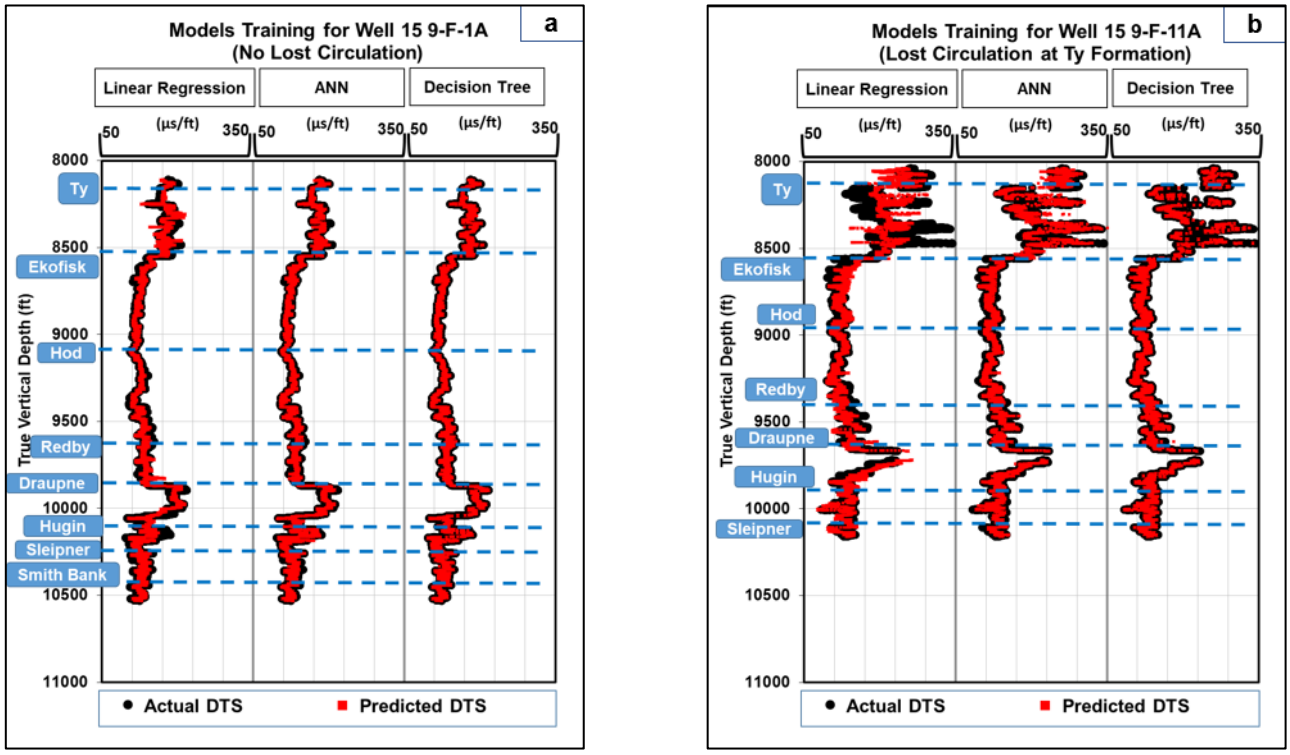

Figure 11: Comparison between the actual DTS and the predicted DTS from the training results of the three ML models for: (a)Well 1A. (b)Well 11A.

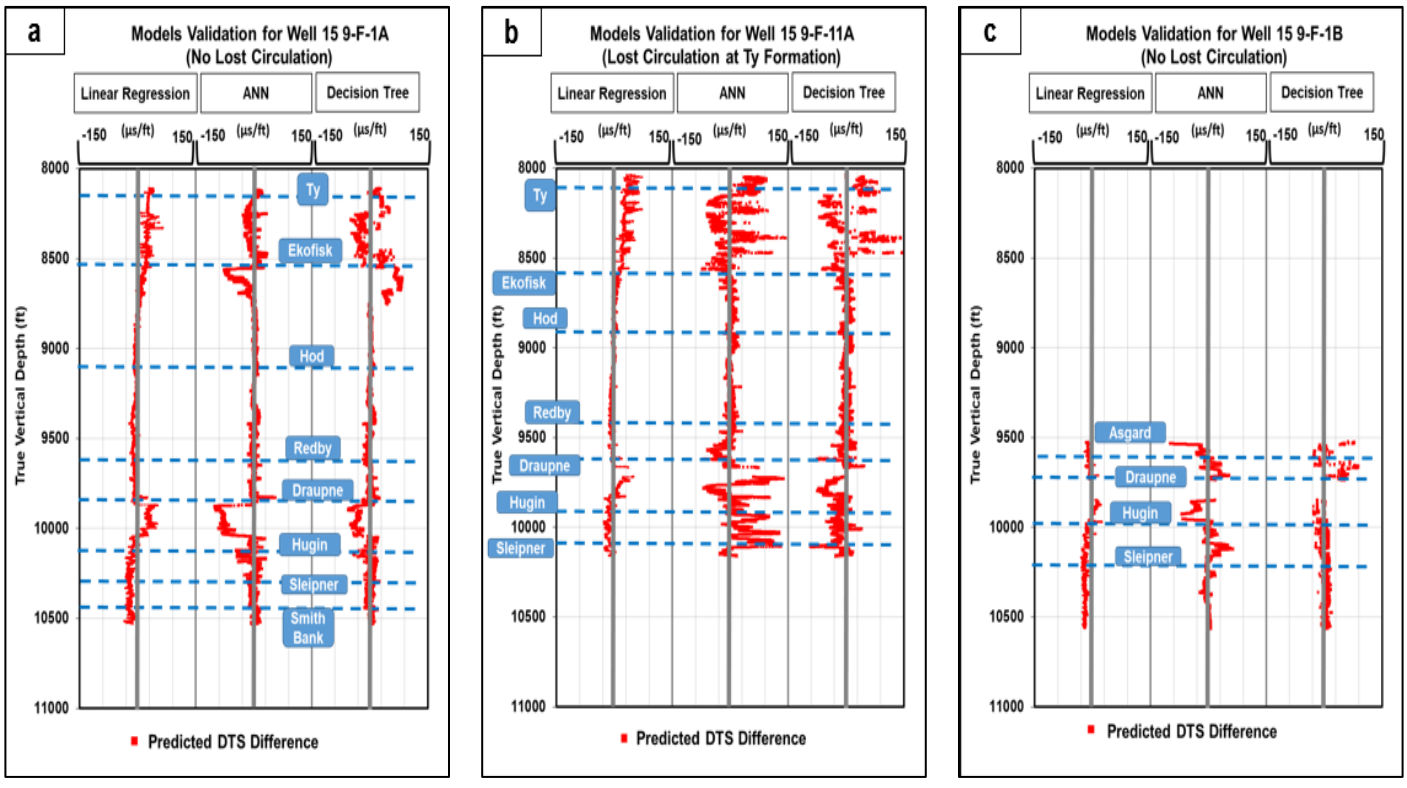

Figure 10: ML models validation based on the difference between the mud loss model (i.e., trained by well 11A dataset) and the no mud loss model (i.e., trained by well 1A dataset). The grey thick vertical lines represent zero difference. (a)Well 1A validation. (b)Well 11A validation. (c)Well 1B validation.

Conclusions

In this study, we developed 3 ML models (i.e., LR, ANN, and DT models) to detect fractured layers, possible mud loss zones, by predicting DTS from conventional well logs of two wells: a well with mud loss (11A) and a well with no mud loss events (1A). A positive DTS difference, DTS from the mud loss model minus the DTS from the no mud loss model, across a specific zone suggests the possible existence of natural fractures based on the shear wave splitting phenomenon.

The feature selection for the developed models showed that the neutron porosity has the strongest correlation with the DTS for the mud loss models, which might be explained by the strong dependency on the fracture porosity in the Ty formation of well 11A. On the other hand, the DTC showed the strongest correlation with DTS for the no mud loss models.

For wells with no evidence of mud loss, wells 1A and 1B, the LR, ANN, and DT models predicted a DTS difference of almost zero or with minimal variance across most formations. However, for well 11A, a well with mud loss events across the Ty formation, both the DT and the ANN models detected layers of high DTS difference of approximately 130 µs/ft, possible fractured zones, across the Ty formation, while the LR model indicated DTS difference of almost zero.

The presented technique and results can be utilized to identify fractured zones to mitigate lost circulation incidents, which would help in better designing and optimizing the drilling operations.

Acknowledgments

The authors would like to thank Equinor and the Volve license partners for the permission to utilize the Volve field data in developing the ML models of this study.

https://www.equinor.com/content/dam/statoil/documents/what-we-do/Equinor-HRS-Terms-and-conditions-for-licence-to-data-Volve.pdf

References

Ahmed, Abdulmalek, Salaheldin Elkatatny, Abdelwahab Ali, and Abdulazeez Abdulraheem. 2020. “Prediction of Lost Circulation Zones Using Artificial Neural Network and Functional Network.” In , D012S116R192. https://doi.org/10.2118/203268-MS.

Al-Hameedi, A. T., S. Dunn-Norman, H. H. Alkinani, R. E. Flori, and S. A. Hilgedick. 2017. “Limiting Drilling Parameters to Control Mud Losses in the Dammam Formation, South Rumaila Field, Iraq.” In , ARMA-2017-0930.

Ameen, Mohammed S. 2014. “Fracture and In-Situ Stress Patterns and Impact on Performance in the Khuff Structural Prospects, Eastern Offshore Saudi Arabia.” *Marine and Petroleum Geology* 50 (February): 166–84. https://doi.org/10.1016/j.marpetgeo.2013.10.004.

Bishop, Christopher. 2006. *Pattern Recognition and Machine Learning (Information Science and Statistics)*. 1st ed.

Brocher, Thomas M. 2005. “Empirical Relations between Elastic Wavespeeds and Density in the Earth’s Crust.” *Bulletin of the Seismological Society of America* 95 (6): 2081–92. https://doi.org/10.1785/0120050077.

Carman, P.C. 1997. “Fluid Flow through Granular Beds.” *Chemical Engineering Research and Design* 75 (December): S32–48. https://doi.org/10.1016/S0263-8762(97)80003-2.

Castagna, J. P., M. L. Batzle, and Raymond L. Eastwood. 1985. “Relationships between Compressional-Wave and Shear-Wave Velocities in Clastic Silicate Rocks.” *Geophysics* 50 (4): 571–81. https://doi.org/10.1190/1.1441933.

Chen, S. T. 1989. “Shear-Wave Logging with Quadrupole Sources.” *Geophysics* 54 (5): 590–97. https://doi.org/10.1190/1.1442686.

Costa, Antonio. 2006. “Permeability-Porosity Relationship: A Reexamination of the Kozeny-Carman Equation Based on a Fractal Pore-Space Geometry Assumption.” *Geophysical Research Letters* 33 (2). https://doi.org/10.1029/2005GL025134.

Gowida, Ahmad, and Salaheldin Elkatatny. 2020. “Prediction of Sonic Wave Transit Times From Drilling Parameters While Horizontal Drilling in Carbonate Rocks Using Neural Networks.” *Petrophysics - The SPWLA Journal of Formation Evaluation and Reservoir Description* 61 (05): 482–94. https://doi.org/10.30632/PJV61N5-2020a6.

Gutierrez, Mario. 2017. “Rock-Physics Modeling of near-Surface Deepwater Sediments for Amplitude Calibration: Application to Shallow Hazard Evaluations.” In , SEG-2017-17326914.

Jahanbakhshi, Reza, and Reza Keshavarzi. 2015. “Quantitative and Qualitative Analysis of Lost Circulation in Natural and Induced Fractured Formations: The Integration of Operational Conditions and Geomechanical Parameters.” *European Journal of Environmental and Civil Engineering* 19 (4): 418–44. https://doi.org/10.1080/19648189.2014.949872.

Jahanbakhshi, Reza, Reza Keshavarzi, and Sajad Jalili. 2014. “Artificial Neural Network-Based Prediction and Geomechanical Analysis of Lost Circulation in Naturally Fractured Reservoirs: A Case Study.” *European Journal of Environmental and Civil Engineering* 18 (3): 320–35. https://doi.org/10.1080/19648189.2013.860924.

Jeirani, Zahra, and Ali Mohebbi. 2006. “Artificial Neural Networks Approach for Estimating Filtration Properties of Drilling Fluids.” *Journal of the Japan Petroleum Institute* 49 (2): 65–70. https://doi.org/10.1627/jpi.49.65.

Katsuki, Daisuke, Marte Gutierrez, and Abdulhadi Almrabat. 2019. “Stress-Dependent Shear Wave Splitting and Permeability in Fractured Porous Rock.” *Journal of Rock Mechanics and Geotechnical Engineering* 11 (1): 1–11. https://doi.org/10.1016/j.jrmge.2018.08.004.

Kholy, S. M., and Hunjoo P. Lee. 2022. “Inferring Compressional Wave (P-Wave) Travel Time from Conventional Well Logs Using Supervised Machine Learning: Case Studies from Texas Basins.” In , ARMA-2022-0461. https://doi.org/10.56952/ARMA-2022-0461.

Koizumi, Carl J. 1988. “Computer Determination of Calibration and Environmental Corrections for a Natural Spectral Gamma Ray Logging System.” *SPE Formation Evaluation* 3 (03): 637–44. https://doi.org/10.2118/14186-PA.

KOZENY, J. 1927. “Uber Kapillare Leitung Des Wassers Im Boden-Aufstieg, Versickerung Und Anwendung Auf Die Bewasserung, Sitzungsberichte Der Akademie Der Wissenschaften Wien.” *Mathematisch Naturwissenschaftliche Abteilung* 136: 271–306.

Moazzeni, A. R., M.. Nabaei, and S. Ghadami Jegarluei. 2010. “Prediction of Lost Circulation Using Virtual Intelligence in One of Iranian Oilfields.” In , SPE-136992-MS. https://doi.org/10.2118/136992-MS.

Muqtadir, Arqam, S. M. Elkatatny, Z. Tariq, M. A. Mahmoud, and A. Abdulraheem. 2019. "Application of Artificial Intelligence to Predict Sonic Wave Transit Time in Unconventional Tight Sandstones." In , ARMA-2019-0036.

Panda, Manmath N., and Larry W. Lake. 1994. "Estimation of Single-Phase Permeability from Parameters of Particle-Size Distribution1." *AAPG Bulletin* 78 (7): 1028–39. https://doi.org/10.1306/A25FE423-171B-11D7-8645000102C1865D.

Rabia, Hussain. 2002. *Well Engineering and Constructions*. Entrac Consulting Limited.

Rajabi, Meysam, Omid Hazbeh, Shadfar Davoodi, David A. Wood, Pezhman Soltani Tehrani, Hamzeh Ghorbani, Mohammad Mehrad, Nima Mohamadian, Valeriy S. Rukavishnikov, and Ahmed E. Radwan. 2022. "Predicting Shear Wave Velocity from Conventional Well Logs with Deep and Hybrid Machine Learning Algorithms." *Journal of Petroleum Exploration and Production Technology*, July. https://doi.org/10.1007/s13202-022-01531-z.

Rodolfo, Soto B., Duarry Arteaga, Cintia Martin, and Freddy Rodriguez. 2010. "The Correct Shale-Volume Characterization Increases Hydrocarbon Reserves: Case Study of Cretaceous Formation, Lake Maracaibo, Venezuela." In , SPE-136811-MS. https://doi.org/10.2118/136811-MS.

Roy, Vishnu, Ankur Gupta, Romy Agrawal, Nitesh Kumar, and Amit Saxena. 2022. "Augmenting and Eliminating the Use of Sonic Logs Using Artificial Intelligence: A Comparative Evaluation." *Geophysical Prospecting* n/a (n/a). https://doi.org/10.1111/1365-2478.13213.

Tillotson, Philip, Jeremy Sothcott, Angus Ian Best, Mark Chapman, and Xiang-Yang Li. 2012. "Experimental Verification of the Fracture Density and Shear-Wave Splitting Relationship Using Synthetic Silica Cemented Sandstones with a Controlled Fracture Geometry." *Geophysical Prospecting* 60 (3): 516–25. https://doi.org/10.1111/j.1365-2478.2011.01021.x.

Toreifi, Hojjat, Habib Rostami, and Abbas Khaksar manshad. 2014. "New Method for Prediction and Solving the Problem of Drilling Fluid Loss Using Modular Neural Network and Particle Swarm Optimization Algorithm." *Journal of Petroleum Exploration and Production Technology* 4 (4): 371–79. https://doi.org/10.1007/s13202-014-0102-5.

Will, Robert, Rosalind Archer, and Bill Dershowitz. 2005. "Integration of Seismic Anisotropy and Reservoir-Performance Data for Characterization of Naturally Fractured Reservoirs Using Discrete-Feature-Network Models." *SPE Reservoir Evaluation & Engineering* 8 (02): 132–42. https://doi.org/10.2118/84412-PA.

Wood, David A. 2020. "Bakken Stratigraphic and Type Well Log Learning Network Exploited to Predict and Data Mine Shear Wave Acoustic Velocity." *Journal of Applied Geophysics* 173 (February): 103936. https://doi.org/10.1016/j.jappgeo.2019.103936.